SAE TECHNICAL
PAPER SERIES

922324

Predicting the Effects of Air and Coolant Temperature, Deposits, Spark Timing and Speed on Knock in Spark Ignition Engines

Sergei Brussovansky, John B. Heywood, and James C. Keck
Massachusetts Institute of Technology

SAE The Engineering Society For Advancing Mobility Land Sea Air and Space®
INTERNATIONAL

International Fuels and Lubricants
Meeting and Exposition
San Francisco, California
October 19-22, 1992

400 COMMONWEALTH DRIVE, WARRENDALE, PA 15096-0001 U.S.A.

922324

Predicting the Effects of Air and Coolant Temperature, Deposits, Spark Timing and Speed on Knock in Spark Ignition Engines

Sergei Brussovansky, John B. Heywood, and James C. Keck
Massachusetts Institute of Technology

ABSTRACT

The prediction of knock onset in spark-ignition engines requires a chemical model for the autoignition of the hydrocarbon fuel-air mixture, and a description of the unburned end-gas thermal state. Previous studies have shown that a reduced chemistry model developed by Keck et al. adequately predicts the initiation of autoignition. However, the combined effects of heat transfer and compression on the state of the end gas have not been thoroughly investigated. The importance of end-gas heat transfer was studied with the objective of improving the ability of our knock model to predict knock onset over a wide range of engine conditions. This was achieved through changing the thermal environment of the end gas by either varying the inlet air temperature or the coolant temperature.

Results show that there is significant heating of the in-cylinder charge during intake and a substantial part of the compression process. The effects of deposits on the combustion chamber walls in promoting knock were also investigated. Their primary effect is a thermal one: since the outer surface temperature of the deposits is hotter than that of the clean engine walls, greater bulk gas heating occurs. However, our results suggest that active species in the end gas carried over from preceding cycles may play a more important role in enhancing knock when deposits are present. Finally, initial work in developing a knock prediction methodology for investigating the audible knock limit of an engine was undertaken. A comparison of the audible knock predictions with the experimental limits as a function of speed is discussed.

INTRODUCTION AND OBJECTIVES

Spark-ignition engine knock is caused by pressure oscillations within the combustion chamber resulting from spontaneous ignition of the end gas which causes rapid energy release and the formation of localized high-pressure regions. Pressure waves propagate from such regions and are reflected back and forth across the cylinder. Temperature and pressure are two important variables in determining whether or not the end gas autoignites. Engine knock limits the compression ratio of an engine, and thus it's efficiency and power output [1].

There exists a need to understand the knock processes in greater detail so that more accurate models can be developed which can be used to assist engine designers. A reduced chemical kinetic model for the autoignition of fuel-air mixtures has been developed recently by Keck et al. [2]. Much work has gone into determining whether or not this reduced chemical model can be a reliable tool in predicting the onset of knock in spark-ignition engines [2,3,4,5,6]. Cowart [4,6] in his study concluded that the chemistry of this reduced kinetic model compares well with that of the much more detailed model developed by Westbrook and Pitz at the Lawrence Livermore National Laboratory [4].

The reduced chemical kinetic model was adapted for use to predict the onset of knock in the end gas in spark-ignition engines by Chun et al. [3,5]. In applying the reduced chemistry model to spark-ignition engines, a model is needed for estimating the state of the region of the end gas most likely to knock. The end gas may not be homogeneous with respect to local differences in temperature, air fuel ratio, residual gas fraction, radicals, intermediate products, etc.. Autoignition will take place in pockets where the conditions in total are the most favorable ones. While the composition of the fuel, air, residual gas, mixture does affect knock occurrence, the mixture temperature is the dominant variable and, in the absence of a pronounced negative temperature coefficient region, it is assumed that the hottest part of the end gas will autoignite first. The modeling objective is to predict the point in time at which this hottest portion of the end gas autoignites thus leading to knock. End-gas non-uniformity has been investigated by König et al. [7,8] who state that exothermic centers or hot spots play an important role in initiating knock. They further say that these exothermic centers arise through temperature and compositional nonuniformity in the end gas [7].

The objectives of this work were:

1) To examine how the thermal environment of the end

gas is affected by heat transfer and gas compression. Experimentally the thermal environment of the end gas was varied through inlet air temperature and coolant temperature changes. By comparing model predictions with experimental results, we were able to examine whether bulk heating and wall heating have similar or significantly different effects on knock onset, due to the different temperature distributions they produce in the end-gas region.

2) To determine the ability of the model to predict knock when deposits on the combustion chamber walls are significant. Again, model predictions were compared with experimental results from a heavily deposited and then cleaned engine to determine whether the effects of deposits on knock were thermal or also affected end-gas composition.

3) To develop an engine simulation methodology for predicting the audible knock limit of an engine. Measured audible knock limits of a multi-cylinder engine over the engine's speed range were compared with model predictions of knock onset.

EXPERIMENTAL APPARATUS AND PROCEDURES

The cylinder pressure data on knock occurrence as a function of inlet air temperature were collected on a single-cylinder Ricardo Hydra research engine [6]. The engine's geometric details as well as the experimental operating conditions are listed in Tables 1 and 2. The temperature of the inlet air was increased above ambient through the use of electrical heaters, and was varied between 25 C and 65 C. The engine operating condition for these experiments was 1500 rpm at wide open throttle (WOT). The fuel used was primary reference fuel 90 (PRF90), a mixture of 90 % isooctane and 10% normal heptane by volume.

Table 1. Ricardo Engine Geometry

Model:	Ricardo Hydra Mark III
Type:	Single Cylinder, cast iron block aluminum alloy head, DOHC
Chamber:	Hemispherical; spark plug 17 mm off center
Fuel Delivery:	Port injection
Bore:	85.7 mm
Stroke:	86.0 mm
Clearance Volume:	69.25 cc
Compression Ratio:	8.3

Table 2. Inlet Air Temperature Experiments

Inlet T (C)	Spark (BTC)	Phi**	RPM*	Fuel
25	26	1.00	1500	PRF90
35	20	1.04	1500	PRF90
45	20	1.06	1500	PRF90
55	20	1.07	1500	PRF90
65	20	1.09	1500	PRF90

*All at WOT: **Phi= equivalence ratio

Pressure data was sampled once per crank angle degree for most of the engine cycle using a Kistler 7061 water-cooled piezoelectric pressure transducer. The pressure transducer signal was set equal to the intake system pressure at bottom center (BC). During knocking combustion the data was fast sampled at the rate of approximately 11 times per crank angle degree to obtain better data resolution. The air flow rate and the fuel flow rate were measured. The air flow rate was determined using a laminar flow element. The fuel was injected into the inlet port using a Bosch fuel injector. The flow rate of the fuel was measured through the use of a buret and stop watch. An oxygen sensor, connected to a NGK lambda meter, was also installed just downstream of the exhaust port. For more detail on the experimental set-up and procedures see Cowart [4,6].

Table 3. Chrysler Engine Geometry

Engine Type:	4 cylinder, 4 stroke, cast iron block, aluminum cylinder head, SOHC
Chamber:	"Fast Burn" design (masked intake valves)
Fuel Delivery:	Throttle body injection
Bore:	8.82 cm
Stroke:	9.1 cm
Clearance Volume:	5.19 cm^3
Compression Ratio:	9.64

Table 4. Experimental Operating Conditions for Varying Coolant Temperature Experiments

T (C)	Spark (BTC)	Phi**	RPM	Fuel
1) With deposits: $T_{ambient}$ = 23 C, T_{air} = 34 C, 90 % of WOT				
41	20	1.01	1900	PRF90
63	20	1.01	1900	PRF90
88	20	1.01	1900	PRF90
105	20	1.01	1900	PRF90
2) Without deposits: $T_{ambient}$ = 35 C, T_{air} = 45 C, 90 % of WOT				
47	20	1.01	1900	PRF90
61	20	1.01	1900	PRF90
96	20	1.01	1900	PRF90
107	20	1.01	1900	PRF90

The cylinder pressure data used to examine the effects of coolant temperature, deposits, spark timing and speed on knock were taken on a Chrysler 2.2 liter, 4-cylinder, production spark-ignition engine. Pertinent engine data are listed in Table 3. The coolant temperature ranged from 41 C to 107 C (Table 4). It was measured on the outlet side of the engine head. The coolant temperature was adjusted using the two heat exchangers which cool the engine oil and the engine coolant. The cooling water to the heat exchangers was throttled to increase the coolant temperature. To decrease

the coolant temperature the engine cooling system was modified from a closed-loop system to an open-loop system.

The engine operating point for the coolant temperature experiments (Table 4) was 1900 rpm at a load of 90 % of the WOT maximum. The fuel used was PRF90. The spark timing of the Chrysler engine was measured using a timing gun. Two sets of data where the coolant temperature was varied were taken, one with substantial deposits on the combustion chamber walls and one without.

The fuel flow rate and the air flow rate were determined as follows. Fuel flow was measured based on given weight of fuel consumed during a specified time. The oxygen sensor, which was located downstream from the exhaust manifold, gave the air-fuel ratio relative to stoichiometric. From these two measurements the air flow rate was then calculated.

Cylinder pressure data were collected from only one cylinder using a Kistler 6121 pressure transducer. Cylinder # 1 was chosen for this purpose, since it was the one that knocked the worst according to Valtadoros's experiments on the same engine [9]. The pressure was fast sampled at the rate of approximately 8 times per crank angle degree, during knocking combustion.

The data which dealt with the audible knock limit of an engine as a function of speed were also collected from the first cylinder of the Chrysler engine. The data were taken at a load of 87 % of the WOT maximum at speeds of 1500 rpm, 1900 rpm, 2200 rpm, and 2500 rpm. Two data sets were collected, one at MBT spark timing and the other one at the audible knock limit spark timing of the engine. The fuel used to obtain the data at MBT spark timing was PRF95. During the audible sessions PRF90 was used. For more details on the engine set-up see Valtadoros [9].

KNOCK MODEL AND ANALYSIS PROCEDURES

The knock model is a computer program which predicts the crank angle at which knock first occurs on an individual cycle basis. The two most important parts of the code are: 1) a thermal state model for calculating the temperature of the hottest part of the end gas, and 2) a chemical kinetic model for determining the sensible energy release rate due to chemical reactions.

In the thermodynamic model it is assumed that during intake and early compression when the mean gas temperature

$$\overline{T} = \frac{p\,V}{mR} \tag{1}$$

is less than the mean wall temperature and the compression rate is low, heating of the unburned gas by the walls will be important. During later compression, when the mean gas temperature exceeds the mean wall temperature, but the compression rate is very high, cooling of the unburned gas will be much slower and we assume that there will be regions of gas, e.g. the cores of turbulent eddies, for which the compression will be adiabatic.

The point in the cycle at which the adiabatic assumption becomes valid can be estimated by comparing the characteristic cooling time for a cylindrical eddy of radius r,

$$\tau_c = \left(\frac{r}{2.4}\right)^2 \Big/ \alpha \tag{2}$$

where α is the thermal diffusivity, with the characteristic adiabatic temperature rise time,

$$\tau_a = \frac{T_a}{\dot{T}_a} = \frac{\gamma}{\gamma - 1}\,\frac{p}{\dot{p}} \tag{3}$$

where γ is the specific heat ratio. When τ_c exceeds τ_a the assumption will be reasonable.

Characteristic eddy radii during the combustion phase of compression have been estimated from measurements of turbulent burning rates [10] and laser sheet photographs [11] and are found to be of order one millimeter.

The relationship between the mean gas temperature and the pressure is obtained from the energy equation applied to the cylinder volume (excluding crevices),

$$\frac{\dot{\overline{T}}}{\overline{T}} = \frac{(\gamma-1)}{\gamma}\frac{\dot{p}}{p} - \frac{\dot{m}_{in}}{m}\left(1 - \frac{T_{in}}{\overline{T}}\right) + \frac{\dot{Q}_T + \dot{Q}_c}{mc_p\overline{T}} \tag{4}$$

where m_{in} is the mass flow rate through the inlet valve, T_{in} is the inlet air temperature, m is the mass in the cylinder, $\dot{Q}_T$ is the rate of heat transfer from the walls to the gas, $\dot{Q}_c$ is the chemical energy release rate, and c_p is the constant pressure specific heat. The three terms on the right side of Eq. (4) represent, respectively, the effects of 1) compression, 2) mixing of fresh charge with residual gas, and 3) heat transfer. Prior to inlet valve close, $\dot{p} = 0$ and the first term is zero; after inlet valve close $\dot{m}_{in} = 0$ and the second term vanishes. Note that Eq. (4) is valid even if there is mass loss from the cylinder and still applies to the unburned end gas during combustion and "knock".

Plots of τ_c, τ_a, and τ_c/τ_a are shown in Fig. 1 for an average burning cycle with a coolant temperature of 100 C and an inlet air temperature of 35 C. Also shown is the dimensionless heat transfer rate $\dot{Q}_T/(mc_p\overline{T})$. It can be seen that at inlet valve close the heat transfer is into the gas and $\tau_c/\tau_a << 1$ so that temperature fluctuations in the gas should be relatively small. At 60 degBTC, the heat transfer changes sign and just slightly later τ_c becomes greater than τ_a. From this point on, τ_c/τ_a increases rapidly, especially during combustion, and conditions are such that, although on the average the end gas is being cooled, the cores of eddies with radii greater than one millimeter are being adiabatically compressed. It is in these cores that we expect chemical reactions leading to knock to proceed most rapidly. The point at which the transition occurs, from more or less uniform

heating to adiabatic compression of eddy cores can not be precisely determined a priori but it is reasonable to expect it to be close to point where the average heat transfer changes sign. This will be discussed in more detail in a later section.

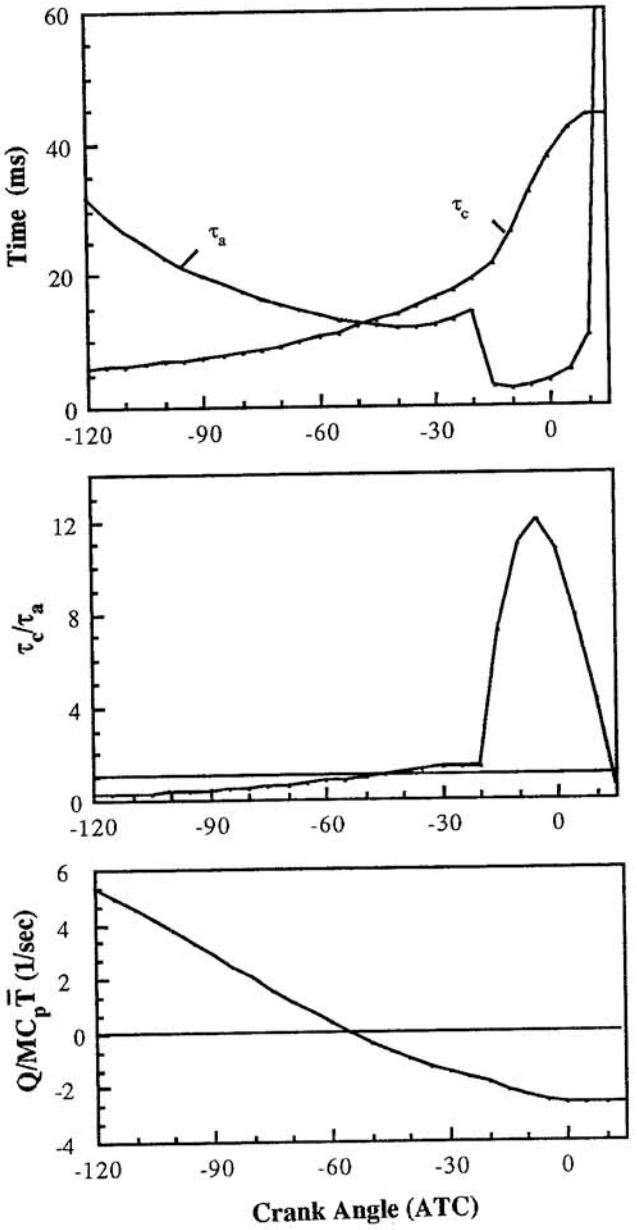

Fig. 1 Adiabatic compression time τ_a, eddy cooling time τ_c, ratio τ_c/τ_a, and heat transfer rate $\dot{Q}/mc_p\bar{T}$ for a representative burning cycle with a coolant temperature of 100 C and an inlet air temperature of 35 C.

An extensive investigation both experimentally and theoretically into the nature of the end gas during knocking combustion was undertaken by König et al. [7,8]. König and co-workers set up two engines with a quartz window which enabled them to take both high-speed Schlieren and natural light cine photography. From their research several conclusions were drawn. One is that end-gas autoignition usually originated at one or more locations within the end-gas region. These "centers", as König et al. call them, grew and often combined leading to larger autoignition regions and finally total ignition of the end gas. Through their work we can conclude that our gas compression model is a simple appropriate approach for estimating the unburned mixture temperature at the point where autoignition originates. If end gas autoignition followed by knock is going to occur, it will initially start at the hottest point within the end gas.

The chemical energy release rate in Eq. (4) is given by

$$\dot{Q}_c = V_u \sum_{i=1}^{n} (-\Delta h_i)\left(R_i^+ - R_i^-\right) \qquad (5)$$

where V_u is the volume of the unburned gas, Δh_i is the enthalpy change for reaction i, n is the number of reactions. The forward and reverse reaction rates per unit volume are given by

$$R_i^{\pm} = k_i^{\pm} \prod_{j=1}^{m} \left[N_j\right]^{\nu_{ji}^{\pm}} \qquad (6)$$

where R_i^+ and R_i^- are the forward and reverse rate constants for reaction i, $[N_j]$ is the concentration of species j, m is the number of species and $\nu_{ji}^{\pm}$ are the forward and reverse stoichiometric coefficients for reaction i. It is a reduced chemistry model and contains 19 reactions and 17 species. The 19 reactions as well as the species names are given in Tables 5 and 6. The model has the ability to predict the two-stage ignition characteristics of hydrocarbon fuels in the low temperature and high pressure region [6]. The knock model can be modified for other fuels by adjusting the reaction constants of the reaction which is most sensitive to the fuel composition. For more information on this see Cowart [6]. For a more complete description of the chemical model see Hu and Keck [2].

Table 5. Reduced Chemical Model of Autoignition [6]
Arrhenius Parameters

Eq.Constant: K = A exp(-E/RT), Rate Constants: k±=exp(-E±/RT)

No. Reaction	A	E/R(10^3T)	ENTHP
1+RH + O2 -> R. + HO2	3.16E13	23.2	46.4
1- R. + HO2. -> RH + O2	1.00E12	0.0	-46.4
2+ R. +O2 -> RO2.	1.00E12	0.0	-31.0
2- RO2. -> R. + O2	2.51E13	13.82	31.0
3+ RO2. -> R.OOH	7.94E11	9.567	7.5
3- R.OOH -> RO2.	1.00E11	5.538	-7.5
4+ R.OOH + O2 -> OO.ROOH	3.16E11	0.0	-31.0
4- OO.ROOH -> R.OOH + O2	2.51E13	13.83	31.0
5+ OO.ROOH -> OROOH + O.H	1.995E11	8.57	-26.6
6+ O.H + RH -> H2O + R.	1.995E13	1.515	-23.5

7+ OROOH -> ORO. + O.H	3.981E15	21.65	43.6
8+ R. + O2 -> C=C + H2O	3.162E11	3.02	-13.5
8- HO2. + C=C -> R. + O2	3.162E11	9.818	13.5
9+ HO2. +HO2. -> HOOH + O2	1.995E12	0.0	-38.5
9- HOOH + O2 -> HO2. + HO2.	1.995E13	19.39	38.5
10+ HOOH + M -> O.H+O.H+M	1.258E17	23.16	51.4
11+ ORO. => R'CHO + R.'	1.00E14	7.55	8.5
12+ R.OOH->C=C+R'CHO+O.H	2.51E14	15.6	-3.0
13+ RO2.+R'CHO->ROOH+R'C.O	2.82E11	4 .35	-0.6
14+ HO2.+R'CHO->HOOH+R'C.O	4.998E11	4 .35	-0.6
15+ C=C + HO2. -> EPOX+O.H	8.88E10	5.0	-0.23
16+ HO2. +RH -> HOOH + R.	5.01E11	8.05	8.0
16- R. + HOOH -> HO2. + RH	6.31E10	4.03	-8.0
17+ RO2. + RH -> ROOH + R.	1.58E11	8.05	8.0
17- R. + ROOH -> RO2. + RH	1.259E10	4.028	-8.0
18+ R. + R. -> RH	1.58E13	0.0	-85.0
19+ RO2. + HO2. -> ROOH+O	21.00E12	0.0	-38.5

Table 6. Reduced Model of Autoignition [6]
Species List

Species #	Model Notation	Species Name
1.	RH	Fuel
2.	O2	Oxygen
3.	R.	Alkyl Fuel Radical
4.	RO2.	Alkylperoxy Radical
5.	.ROOH	Hydro Peroxy Alkyl Radical
6.	.OOROOH	
7.	ORO. (= RO.)	
8.	HO.	Hydroxyl Radical
9.	HO2.	Hydro Peroxy Radical
10.	HOOH	Hydrogen Peroxide
11.	ROOH	Alkyl Hydro Peroxide
12.	RCHO	Aldehyde
13.	C=C	Olefin
14.	R.'	Small Fuel Radical
15.	R'C.O	Acyl Radical
16.	epox	Epoxide (RCH-CH2O)
17.	H2O	Water

Notes:
ROOH and OROOH are assumed identical
R'C.O and epox are assumed inactive
R.' is assumed inactive
RO2. and ORO. are different

In the adiabatic compression region, Eq. 4 reduces to

$$\frac{\dot{T}}{T} = \left(\frac{\gamma-1}{\gamma}\right)\frac{\dot{p}}{p} + \frac{1}{\rho c_p T}\sum_{i=1}^{n}\left(-\Delta h_i\right)\left(R_i^+ - R_i^-\right) \quad (7)$$

The integration of Eq. (7) starts when the heat transfer changes sign. The criteria for best determining the starting place for the adiabatic calculation will be addressed in the next section. The initial cylinder-average temperature is calculated from the ideal gas law, Eq. (1), applied to the entire cylinder part-way through the compression stroke. It depends on the measured cylinder pressure, the cylinder volume and the mass of gas within the cylinder. This mass is the sum of the air, fuel and residual gas masses within the cylinder at intake valve closing. The residual gas mass is estimated from a correlation by Fox [12] based on measurements by Galliot et al. [13]. An accurate value of the initial mass is needed for an accurate estimate of the initial temperature.

The calculated temperature of the end gas obtained from Eq. (7) is used to determine knock occurrence. When the modeled temperature of the unburned gas rises above 1200 K, knock onset is predicted. After this point, the temperature of the end gas is rising at a very high rate representative of the energy release associated with autoignition. Other criteria such as a temperature rise rate of 6×10^6 K/s have been used [6]. A better measure of knock occurrence would be to compare the acoustic time, that is the time it takes for a sound wave to propagate across the combustion chamber, with a chemical time where

$$\tau_{ac} = \frac{Bore}{\sqrt{\gamma R T_{burned}}} \quad (8)$$

and

$$\tau_{chem} = \left(\frac{1}{T}\frac{dT}{dt}\right)^{-1} \quad (9)$$

When the chemical time becomes shorter than the acoustic time, pressure waves are generated since there is not enough time to equilibrate the pressure. By assuming that the pressure rise in the end gas occurs at constant volume, we can develop a relationship between the pressure rise and the two characteristic times as follows:

$$\frac{\Delta p_{end}}{p} = \frac{\Delta T_{end}}{T} = \frac{1}{T}\frac{dT}{dt}\bigg|_v \tau_{ac} = \frac{\tau_{ac}}{\tau_{chem}} \quad (10)$$

Equation (10) says that the pressure rise the end gas experiences is the ratio of the acoustical time to the chemical time. Using any of these criteria the model predicts knock occurrence with differences of less than one crank angle degree [6].

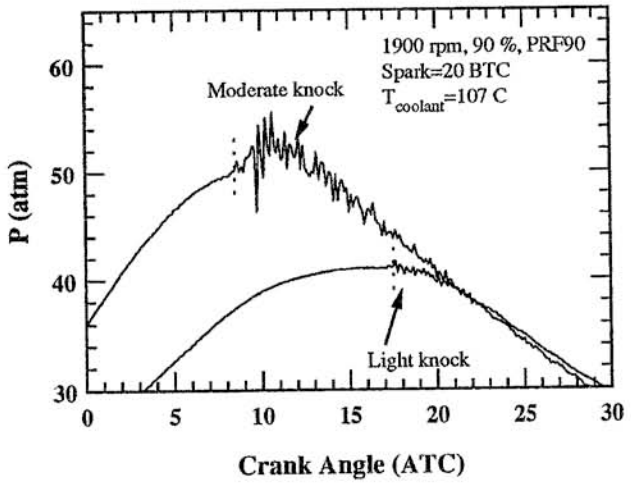

Fig. 2 Knocking combustion pressure traces. Taken from a Chrysler 2.2 liter engine at 1900 rpm, 90 %, spark = 20 BTC using PRF90

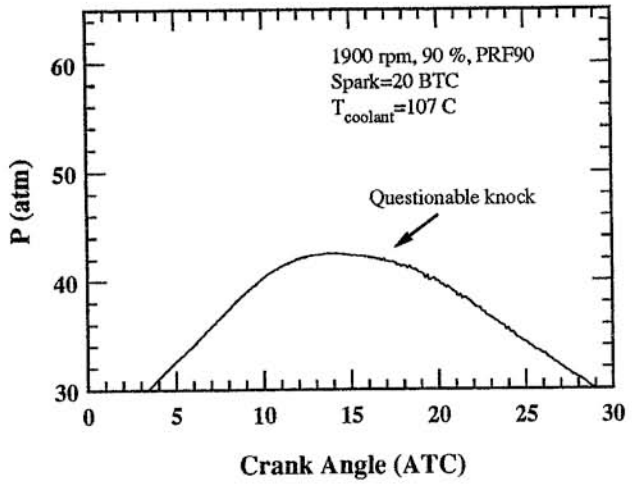

Fig. 3 Non-knocking pressure trace. Taken from a Chrysler 2.2 liter engine at 1900 rpm, 90 %, spark = 20 BTC using PRF90

Typical knocking and non-knocking pressure traces are shown in Fig. 2 and Fig. 3. The objective experimental criterion used to determine knock occurrence was based on a calculation of the rate of change of pressure with respect to the crank angle ($\Delta p/\Delta\theta$) between two successive sample points. If ($\Delta p/\Delta\theta$) exceeded a value of 2.8 atm/degCA, roughly three times the maximum rate of pressure rise during normal burning, then knock was assumed to have occurred. It was on this basis that the traces in Fig. 2 and Fig. 3 were cataloged.

Visual inspection shows that in the case of Fig. 2, this criterion appears satisfactory. However in the case of Fig. 3, visual inspection shows that although the objective criterion for knock was not met, small amplitude oscillations were indeed present and whether this should be considered knock is questionable. At the threshold of audible knock a fairly large fraction of pressure traces fall into the category of Fig. 3 making it difficult to determine either knock crank angles or the fraction of cycles knocking. In addition a determination of the frequency of the oscillations, 40,000 Hz indicates that they are not acoustical oscillations which should have a dominant frequency of approximately 6-10 kHz [14] but more likely ringing of the pressure transducer at its cut off frequency. Averaging out the high frequency oscillations does show the presence of oscillations at the expected acoustical frequency but their amplitude Δp_{ac} is small, of order 0.5 atm in the moderate knock case.

For acoustical oscillations the ratio of the acoustical to the thermal energy is given by

$$\frac{e_{ac}}{c_v T} = \frac{\gamma - 1}{2}\left(\frac{\Delta p_{ac}}{p}\right)^2 \qquad (11)$$

Using Eq. (11) and an estimated value of 0.15 for the unburned mass fraction at knock, it is found that the acoustical energy is of order 10^{-4} of the available chemical energy. Furthermore since the averaged traces show little if any pressure jump at the knock angle, it appears that only a very small portion of the charge autoignites or that the reactions are quenched before completion. The latter could occur if only the first stage reactions but not the second were involved.

The general conclusion is that, while pressure traces of the type shown in Fig. 2 and Fig. 3 can be used to detect the onset of some kind of chemical activity in the end gas, the magnitudes of the energy release and its interpretation, particularly at the audible knock threshold is uncertain.

Once the measured knock onset angle has been determined, the experimental cylinder pressure data is submitted to the knock model, also on an individual cycle basis. This pressure data accounts for the compression-produced temperature rise that the end gas experiences during compression and combustion. Cycles analyzed were selected to provide as wide a range of knock occurrence angle as possible. Experimental and predicted angles of knock onset are then compared. Note that if knock has not been predicted by the time the pressure data indicates knock has occurred, the prior-to-knock pressure data is extrapolated to avoid "triggering" the knock prediction. The pressure data is extrapolated using a least squares fit to the 80 to 180 (depending on the knock occurrence angle) data points prior to the onset of knock.

The data which examine the effects of speed and spark timing on knock prediction were processed differently. The objective was to develop a methodology which could be used to predict the audible knock limit of an engine. At each speed at MBT spark timing, a representative cycle was

chosen which was used to calibrate an engine cycle simulation program. A representative cycle was one which had the average maximum pressure at the average crank angle at which the maximum pressure occurred. The engine simulation and calibration processes are explained by Poulos [15]. After the calibration had been completed, the spark timing within the simulation was varied and the pressure traces thereby obtained from the simulation were submitted to the knock model, which was modified to accept the simulated trace. A series of graphs were generated of predicted knock occurrence versus spark which are discussed in a later section.

EXPERIMENTAL VERSUS PREDICTED KNOCK OCCURRENCE AND THERMAL MODEL ANALYSIS

In this section the cylinder pressure data where the inlet air temperature and the coolant temperature (deposited and clean engine) were varied are analyzed as described previously. Figure 4 shows measured knock versus predicted knock occurrence in degrees after top center (degATC), for the varying inlet air temperature data. Each symbol on the graph represents one cycle from a data set. The solid line at 45 degrees represents predictions matching the measurements. Around 10 cycles from each inlet temperature data set were analyzed and plotted. The spread in knock occurrence angle at each inlet temperature is about 15 crank angle degrees. The predicted knock occurrence angle compares well with the measured knock occurrence angle. The discrepancy between measured and predicted knock onset is a few crank angle degrees.

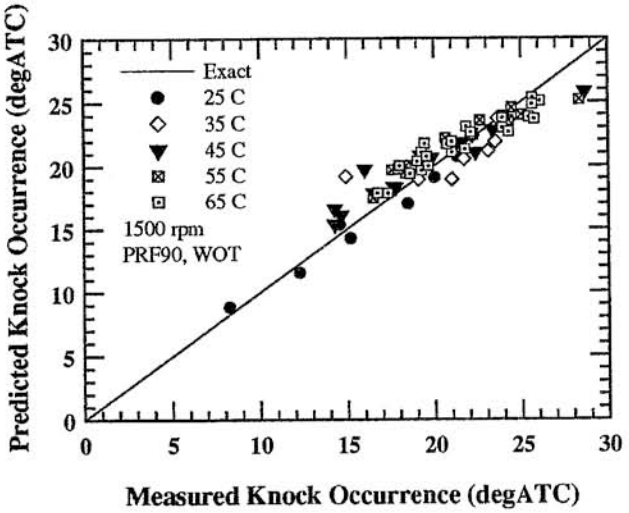

Fig. 4 Measured versus predicted knock occurrence for various inlet temperatures. Adiabatic compression starts at 90 degBTC. At 25 C spark timing = 26 BTC, all others 20 BTC.

The graphs of measured versus predicted knock occurrence show the end result of an extensive calculation sequence. It is important to examine how the end-gas temperature based on the assumption of adiabatic compression once charge heating has ceased compares with the ideal-gas-law derived temperature which is the cylinder-average value. Figure 5 shows a typical unburned-charge temperature history calculated by the knock model (the solid line) compared with the ideal-gas-law temperature (the dotted line). For both models the input is the experimentally measured cylinder pressure. The ideal-gas-law temperature is valid from intake valve closing (IVC) up until spark. The knock model calculation was started at 90 degrees before top center (degBTC), since prior estimates indicated that at about this point during the compression stroke the heat transfer between the gas in the cylinder and the walls changes sign.

As discussed earlier, during the intake process, the walls heat the cylinder contents; then at some time during compression the heat transfer reverses sign and the walls cool the gas. The combustion chamber walls-- piston, cylinder head, valves, and cylinder liner-- are all at different temperatures. The discussion here relates to when the aggregate heat transfer reverses direction. Both models give essentially the same end-gas temperature indicating that for this engine, from 90 degBTC to spark, heating and cooling effects are small. For the varying air temperature data set, knock onset behavior predicted by the model agrees with the experiment.

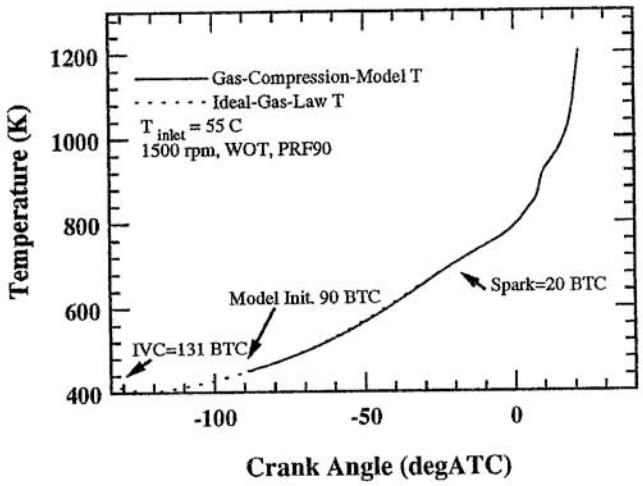

Fig. 5 Comparison of the calculated adiabatic compression model temperature and the ideal-gas-calculated cylinder-average temperature for the data where the inlet temperature was varied. Adiabatic compression starts at 90 degBTC.

The varying coolant temperature data will now be examined. In Fig. 6, a similar graph of unburned charge temperature versus crank angle for one cycle of the cylinder pressure data set from the Chrysler 4-cylinder engine is shown. From 90 degBTC to spark, the positions of the ideal gas law and the adiabatic compression model temperatures are intuitively incorrect. The adiabatic compression model is initialized at the ideal-gas-law temperature. It then drops below the ideal-gas-law prediction. If the hottest part of the end gas is adiabatically compressed than at the least the curves should line up with each other. The most plausible explanation for this trend is charge heating. The adiabatic compression calculation has apparently been started before

charge heating has ceased. To test this hypothesis, the start of the adiabatic compression calculation was moved to a later crank angle of 60 degBTC. The results are shown in Fig. 7; the unburned charge temperature curves now line up in the expected manner. The ideal-gas-law temperature is below the adiabatic gas compression temperature after about 40 degBTC, presumably due to heat loss to the walls.

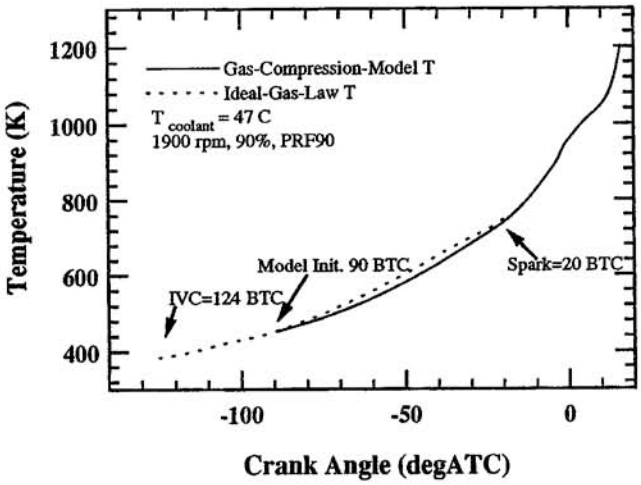

Fig. 6 Comparison of the calculated adiabatic compression model temperature and the ideal-gas-calculated cylinder-average-temperature for the data where the coolant temperature was varied. Adiabatic compression starts at 90 degBTC.

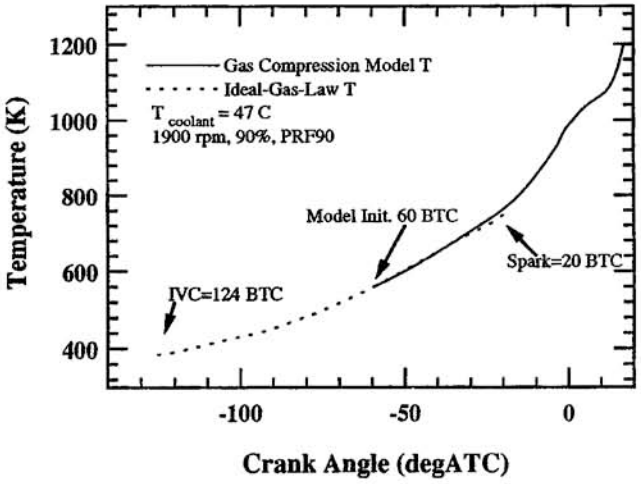

Fig. 7 Comparison of the calculated adiabatic compression model temperature and the ideal-gas-calculated cylinder-average-temperature for the data where the coolant temperature was varied. Adiabatic compression starts at 60 degBTC.

It is obviously important to get accurate estimates of the initial temperature, it is also important to determine where to start the adiabatic compression calculation. An engine simulation based on Eq. (1) and Eq. (4) was used to find the point during compression when the heat transfer changes sign, since it calculates the heat transfer into or out of the cylinder at every crank angle. This method was applied to the high and low coolant temperature data sets with and without deposits. For the clean engine the aggregate heat transfer changes sign at 86 degBTC for the low coolant temperature, and at 79 degBTC for the high coolant temperature. For the case with deposits, it is 79 degBTC and 72 degBTC respectively. All of these angles are later than the 90 degBTC which had previously been used as a starting point for all knock model calculations. Figure 7 shows it does not matter exactly where one starts the calculation as long as it is before either significant end-gas heat loss or chemical energy release in the end gas occur.

Attention will now be focused on knock prediction when varying the coolant temperature. In Fig. 8 the measured knock occurrence angle is plotted versus the predicted knock occurrence angle for the cylinder pressure data set obtained from the clean engine. The adiabatic compression calculations in this case were started at 90 degBTC. The model predicts the onset of knock with reasonable accuracy except for those cycles which knock late in the combustion process where the spread about the 45 degree line increases. The reason for this is the difficulties discussed in connection with Fig. 2 and Fig. 3 of determining the knock crank angle in cases of light knock and questionable knock. When these marginal knocking cycles were visually examined, knock onset could not be precisely determined.

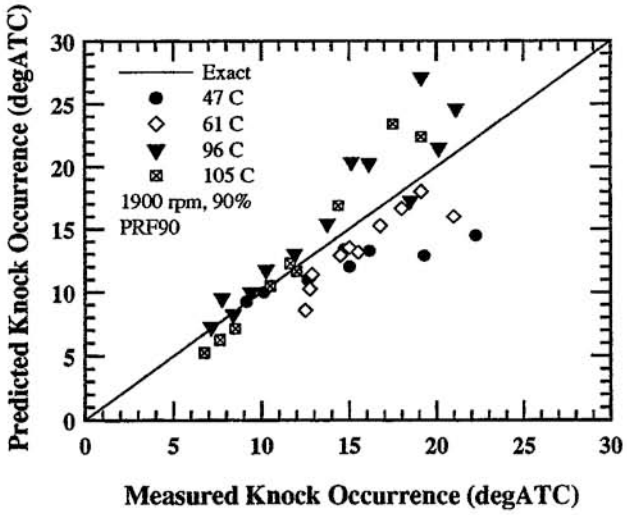

Fig. 8 Measured versus predicted knock occurrence for various coolant temperatures (clean engine). Adiabatic compression starts at 90 degBTC.

Figure 9 shows the end-gas temperature predicted by the knock model with and without chemistry release for one cycle of the high coolant temperature data. It can be seen that heating due to chemical reactions become important just after TC when the core temperature rises above 1150 K. This is just about the limit of validity of the present reduced chemical kinetic model used to predict knock. Work on extending the model to higher temperatures is currently in progress and will be reported later.

We will now discuss the knock onset data and predictions with the heavily deposited engine. The deposits on the combustion chamber and piston were accumulated by continuously cycling the engine between two operating points; 1200 rpm at 10 % load and 2500 rpm at 30 % load. They caused about a 10 octane number increase in the octane requirement of the engine. For more details see Valtadoros [9]. Figure 10 presents the knock onset predictions for the varying coolant temperature data sets with heavy deposits on the combustion chamber walls, when the adiabatic compression model is started at 60 degBTC. The agreement

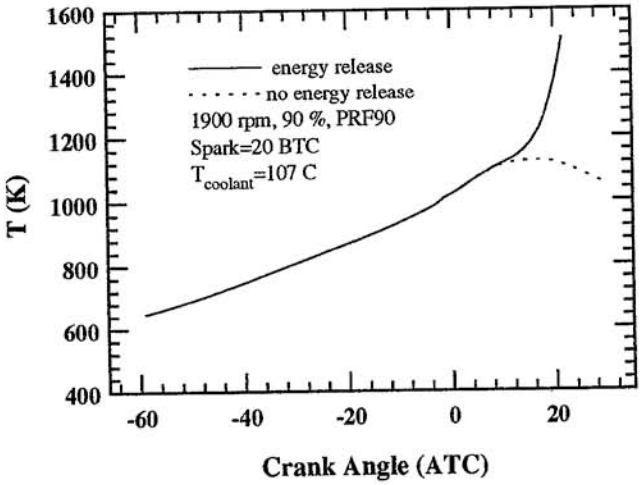

Fig. 9 Predicted end-gas temperature with chemistry energy release and with zero chemistry energy release.

is poor and the points are scattered. The points which are shown on the 30 degATC predicted line in Fig. 10 are cases when the model did not predict knock occurrence. With normal combustion timing, the chances of knock occurring after 30 degATC are very low. The results when deposits are present are unsatisfactory. That the thermal model seems to be behaving well is demonstrated by the inlet temperature data and the coolant temperature data from the clean engine. What role could deposits play in enhancing knock?

The most widespread view is the thermal effect. Because the outer temperature of the deposits (760 K) on the combustion chamber walls is significantly higher than that of the clean chamber walls (580 K), there is greater gas heating [9]. This increases the temperature of the unburned gas during intake and the first part of compression thus promoting knock. Previous experiments in our laboratory with ceramic coated valves and with heated sections of wall [4] indicated that the effect of hot walls on knock was largely due to bulk end-gas heating and not due to localized pockets of hotter gas that stayed in contact with these surfaces throughout compression. It is accepted that deposits increase the compression ratio through the reduction in clearance volume, but this effect is small. One further argument advanced is that deposits increase the concentration of reactive species in the end gas.

The first effect is included in the knock model since it uses the experimental pressure to determine the charge temperature after compression stroke heating ceases. The second effect has been experimentally proven to be small [9]. This leads into the last suggestion: can deposits have a chemical effect in inducing knock, and if they do, what species could be most important? Rapid compression machine experiments done at MIT [16], suggest that residual reactive species (for example hydrogen peroxide) carried over on the walls from one cycle to the next can reduce ignition delays. The solution to this problem in the case of the rapid compression machine was to interlace fuel/air compression's with pure oxygen compression's. The effect could not be eliminated by inert gas compression's or simple purging. Presumably high temperature oxygen was required to oxidize what ever active species were being adsorbed on the walls.

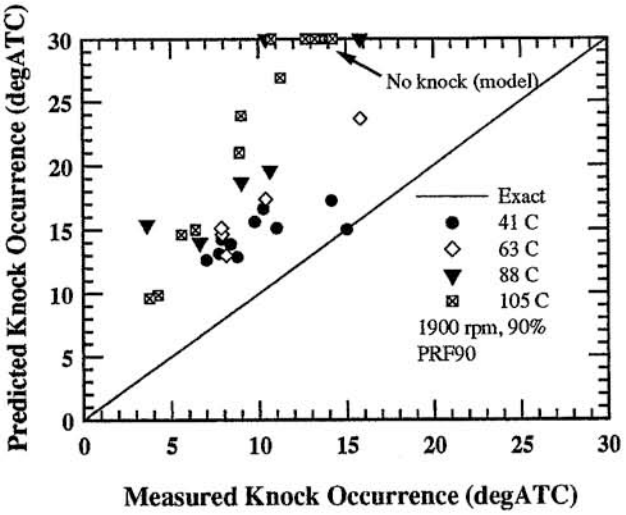

Fig. 10 Measured versus predicted knock occurrence for various coolant temperatures (deposited engine). Adiabatic compression starts at 60 degBTC.

Of the various relatively stable active species present in combustion products which could be carried over from one cycle to the next in the gas phase on the walls, only hydrogen peroxide (H_2O_2) is present in sufficient concentrations to cause an effect in the present kinetic model. Other possibilities which were considered were alkylperoxides and aldehydes but their concentrations in combustion products were many orders of magnitude too small to be important. Nitrogen oxides could also play a role but since the present kinetic model does not include these species it was not possible to investigate them. H_2O_2 was therefore chosen for the present preliminary model studies.

To determine the levels of H_2O_2 which could be present in the combustion products, Stanjan [17], a PC-based equilibrium code, was used. For various combustion product temperatures, the program was run to determine the amount of gas-phase H_2O_2 in the combustion products. The results of these calculations are shown in Fig. 11 where the mole fraction of H_2O_2 is plotted against combustion product temperature. The amount of H_2O_2 varies from 10^{-9} mole fraction to about 10^{-5} mol fraction at high temperature,

where it levels off. The results are not especially sensitive to pressure.

For the low and the high coolant temperature data sets, a sensitivity study was carried out to determine what initial level of H_2O_2 in the end gas gave the best knock onset prediction fit to the experimental data. A linear variation with the coolant temperature was then assumed and the initial levels of H_2O_2 for the intermediate coolant temperatures are shown in Fig. 12. The increasing level of initial H_2O_2 concentration in the end gas with increasing coolant temperature is a plausible trend because the concentrations of H_2O_2 in the combustion products increase with temperature.

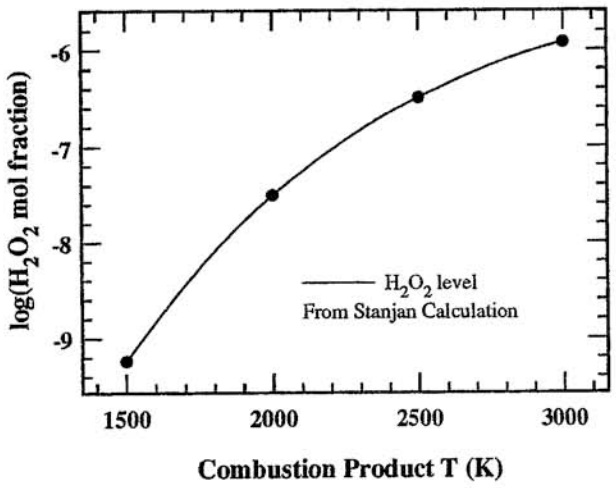

Fig. 11 Hydrogen peroxide concentration as a function of combustion product temperature. Pressure = 50 atm; stoichiometric mixture.

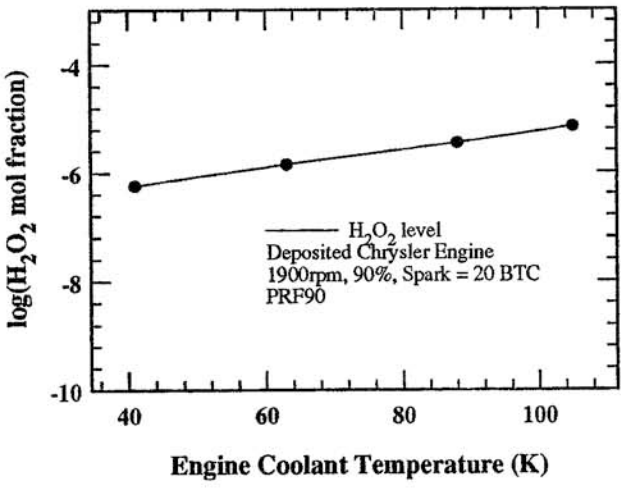

Fig. 12 Fitted hydrogen peroxide concentration versus coolant temperature.

The knock prediction results with these initial levels of H_2O_2 are shown in Fig. 13 for the highest coolant temperature data set. The adiabatic compression calculation is started at 60 degBTC. The circles represent predictions with no initial level of H_2O_2. The squares represent predictions with initial levels of H_2O_2. Inclusion of plausible initial levels of H_2O_2 produces an extremely good fit between prediction and measurement. Figure 14 is a cumulative plot of all coolant temperatures from the data set with deposits, with the appropriate initial H_2O_2 level. This is a much improved match than that of Fig. 10. This exploratory analysis suggests that deposits could enhance knock through their effect on the radical concentration in the end gas, as well as their significant effect on unburned charge heat transfer.

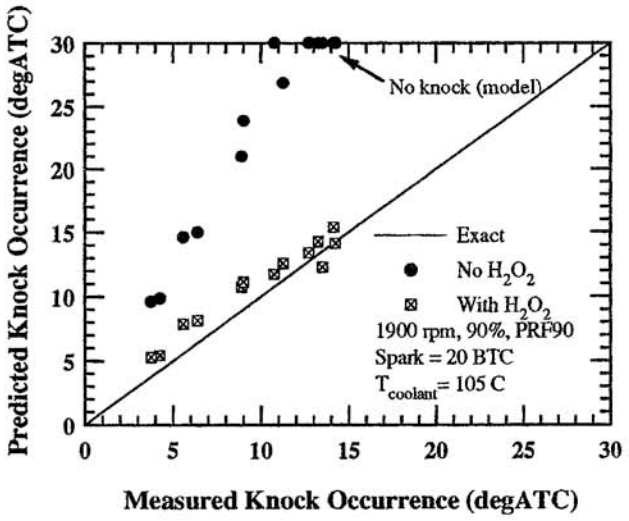

Fig. 13 Measured versus predicted knock occurrence for the high coolant temperature data from the engine containing deposits. Results are shown with and without initial level of hydrogen peroxide in the end gas. Adiabatic compression starts at 60 degBTC.

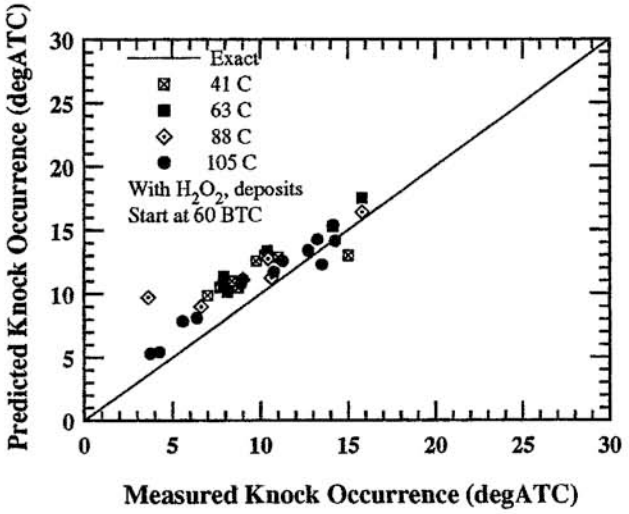

Fig. 14. Measured versus predicted knock occurrence for various coolant temperatures (deposited engine) with the appropriate initial levels of hydrogen peroxide. Adiabatic compression starts at 60 degBTC.

INVESTIGATING ENGINE KNOCK LIMITS

In this section an approach is developed which can be used to predict the knock limits of an engine. Up to this point, the experimental pressure data in a knocking engine were used to determine the end-gas thermal state. The experiments and predictions described in this section, examine the predictive capability of the knock model. The objective was to, based on cylinder pressure data obtained from a cycle simulation rather than use the experimental pressure curve predict the audible knock limit of an engine.

Figure 15 shows the experimental results. The solid line is the MBT spark-timing curve, obtained with 95 octane primary reference fuel (PRF95) at a load of 87 % of the WOT maximum. The dashed line is the spark timing at the measured audible knock limit with a 90 octane primary reference fuel (PRF90). At the lower speeds, audible knock occurs at a spark timing retarded from MBT. As the speed increases, spark timing has to be advanced beyond MBT timing to obtain knock. These results are as expected.

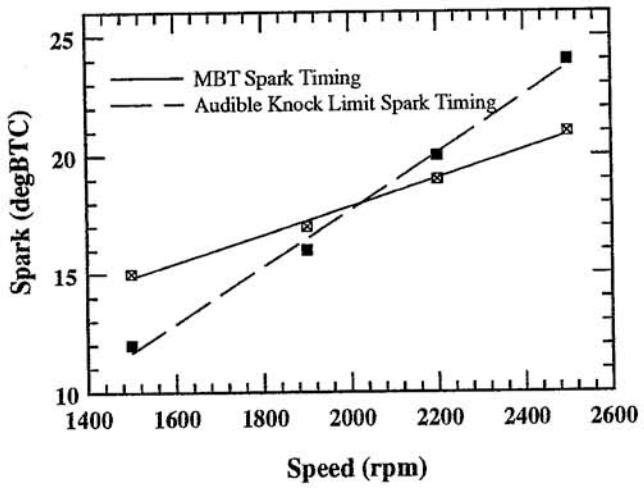

Fig. 15 Experimental results for the audible knock experiments. MBT spark timing and audible knock limit spark timing versus engine speed. Load equals 87% of the WOT value; stoichiometric mixture.

Figure 16 shows that the average measured knock occurrence angle at the audible limit, moves closer to top center as speed increases. Experimentally about thirty percent of the cycles were knocking at the audible knock limit, in agreement with Valtadoros's data [9] who concluded that between twenty to forty percent of the cycles knock at the audible knock limit.

At each speed, after the engine simulation had been calibrated with the MBT data to get the burn parameters correct, the plot in Fig. 17 was developed. It shows spark timing versus predicted knock occurrence for 1500, 1900, 2200 and 2500 rpm. As the spark timing is advanced knock occurs earlier. The vertical line in each plot represents the spark timing when the model no longer predicts knock to occur. For each speed, the spark timing when the predicted knock occurrence crank angle equaled the measured average knock occurrence angle was determined. Table 7 compares the experimentally measured spark timing to the spark timing at which point the knock model predicted the crank angle of average knock occurrence. The results are in good agreement: the knock model is able to predict the audible knock limit of an engine reasonably well. To develop a more accurate predictive methodology, knowledge of how the actual average knock occurrence crank angle behaves at the audible knock limit is needed.

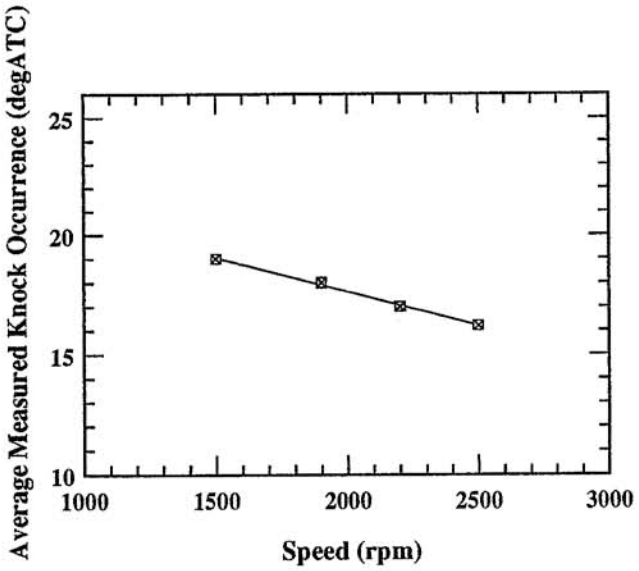

Fig. 16 Average measured knock occurrence angle versus speed.

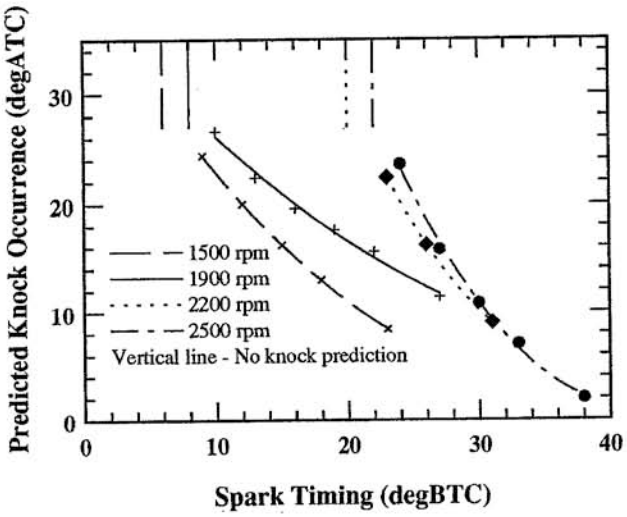

Fig. 17 Knock occurrence angles predicted by the engine cycle simulation versus spark timing, for 1500, 1900, 2200 and 2500 rpm at a load of 87 %. Vertical line indicates knock is not predicted to occur by the knock model.

Table 7. Summary of Audible Knock Experiments and Prediction

rpm	θ_{knock} exp. (ATC)	θ_{spark} pred. (BTC)	θ_{spark} exp. (BTC)	MBT Timing (BTC)	% Cycles Knocking
1500	19.0	12	12	15	28
1900	18.0	18	16	17	42
2200	17.0	24	20	19	33
2500	16.2	26	24	21	29

CONCLUSIONS

1) The validity of a model for the end-gas state -- charge heating followed by adiabatic compression once aggregate heat transfer reverses direction -- has been investigated both experimentally and theoretically. The thermal environment of the end gas was varied through inlet air temperature changes and coolant temperature changes. The results of the analysis show that during intake and compression, significant heating of the in-cylinder charge occurs. The knock model assumes adiabatic compression from the point in time during compression when the aggregate heat transfer with the combustion chamber walls changes direction (from-the-walls, to, to-the-walls). This is the simplest appropriate model for predicting the temperature of the hottest part of the end gas.

2) For the conditions studied here, the aggregate heat transfer reverses direction according to the cycle simulation results at between 85 and 70 degBTC. Initializing the adiabatic compression process just after this reversal point was found to be an appropriate starting point.

3) The primary influence of deposits on the combustion chamber walls in enhancing knock onset is their thermal effect. Because the outer surface temperature of the deposits is significantly higher than that of the clean engine there is greater bulk gas heating. However our analysis of the knock onset data taken in an engine containing substantial deposits suggest that the presence of significant levels of radicals in the end gas may play a role in promoting knock when deposits are present. Including plausible levels of hydrogen peroxide in the initial fuel, air and residual gas mixture brought the comparison of predicted knock onset into good agreement with the measured value for knock occurrence.

4) An approach for predicting the audible knock limit of an engine over its speed range has been developed. Using pressure traces predicted with an engine cycle simulation, the knock model is able to predict the audible knock limit of an engine reasonably well. This methodology does require knowledge of how the actual average knock occurrence angle varies with speed at the audible knock limit.

ACKNOWLEDGMENT

This work has been supported by the Sloan Automotive's Laboratory's Consortium for Engine Research. Members are: Chrysler Corporation, Ford Motor Company, Peugeot Societe Anonyume, Regie National des Usines Renault, and Volvo Car Corporation.

REFERENCES

1. Heywood, J.B., Internal Combustion Engine Fundamentals, McGraw-Hill Book Co., 1988.

2. Hu, Haoran, Keck, James, "Autoignition of Adiabatically Compressed Gas Mixtures," SAE paper 872210, SAE Trans., vol. 96, International Fuels and Lubricants Meeting, Toronto, Ontario, Canada, November 2-5, 1987.

3. Chun, K.M., "Characterization of Knock and Prediction of its Onset in a Spark-Ignition Engine," PhD Thesis, Department of Mechanical Engineering, MIT, 1988.

4. Cowart, J.S., Keck, J.C., Heywood, J.B., Westbrook, C.K. and Pitz, W.J.: "Comparison of Engine Knock Predictions Using a Fully-Detailed and a Reduced Chemical Kinetic Mechanism," Paper presented at the Western States Section of the Combustion Institute, Livermore, CA, October 23-24, 1989.

5. Chun, K.M., Heywood, J.B., Keck, J.C., "Prediction of Knock Occurrence in a Spark Ignition Engine," Proceedings of the 22nd Symposium (International) on Combustion, The Combustion Institute, pp. 455-463, 1988.

6. Cowart, Jim S., "Predicting Knock Onset in a Spark Ignition Engine," S.M. Thesis, Department of Mechanical Engineering, MIT, 1990.

7. König, G., Maly, R.R., Bradley, D., Lau, A.K.C. and Sheppard, C.G.W., "Role of Exothermic Centers on Knock Initiation and Knock Damage," SAE paper 902136, Paper presented at the International Fuels and Lubricants Meeting and Exposition, Tulsa, Oklahoma, October 22-25, 1990.

8. König, G., Sheppard, C.G.W., "End Gas Autoignition and Knock in a Spark Ignition Engine," SAE paper 902135, Paper presented at the International Fuels and Lubricants Meeting and Exposition, Tulsa, Oklahoma, October 22-25, 1990.

9. Valtadoros, Tassos H., "Fuel Additive Effects on Deposit Buildup and Knock in a Spark Ignition Engine," S.M. Thesis, Department of Mechanical Engineering, MIT, 1990.

10. Keck, J. C., "Turbulent Flame Structure and Speed in Spark Ignition Engines," 19th Symposium (International) on Combustion, 1451, 1987.

11. Zur Loye, A. D., Braces, F. V., "Two-Dimensional Visualization of Premixed-Charge Flame Structure in an IC Engine," SAE paper 870454, 1987.

12. Fox, Jonathan W., "Effects of Fuel Injection Strategy on HC Emissions During SI Engine Start-Up," S.M. Thesis, Department of Mechanical Engineering, MIT, 1992.

13. F. Galliot, W.K. Cheng, C-O Cheng, M. Sztenderowicz, J. B. Heywood, and N. Collings, "In-Cylinder Measurements of Residual Gas Concentration in a Spark Ignition Engine," SAE paper 900485, The Society of Automotive Engineers, 1990.

14. Haghgooie, M., "Effects of Fuel Octane Number on Knock Characteristics of a Single Cylinder Engine," SAE paper 902134, 1990.

15. Poulos, Stephen G., "The Effect of Combustion Chamber Geometry on S.I. Engine Combustion Rates-A Modeling Study," SAE paper 830334, Paper presented at the International Congress and Exposition, Detroit, Michigan, February 28-March 4, 1983.

16. Park, P., Keck, J. C., "Rapid Compression Machine Measurements of Ignition Delays for Primary Reference Fuels," SAE paper 900027, 1990.

17. Reynolds, Wm. C., *Stanjan chemical equilibrium solver*, Stanford, CA, 1987.